Vision Research 164 (2019) 24–33

Contents lists available at ScienceDirect

Vision Research

journal homepage: www.elsevier.com/locate/visres

Vertical size disparity induces enhanced neural responses in good stereo observers

Hiroyuki Mitsudo[a,*], Naruhito Hironaga[b], Katsuya Ogata[b], Shozo Tobimatsu[b]

[a] Division of Psychology, Department of Human Sciences, Faculty of Human-Environment Studies, Kyushu University, 744 Moto-oka, Nishi-ku, Fukuoka 819-0395, Japan
[b] Department of Clinical Neurophysiology, Neurological Institute, Faculty of Medicine, Graduate School of Medical Sciences, Kyushu University, 3-1-1 Maidashi, Higashi-Ku, Fukuoka 812-8582, Fukuoka, Japan

ARTICLE INFO

Keywords:
Alpha-band phase locking
Binocular disparity
Stereopsis
Magnetoencephalography
Visual cortex

ABSTRACT

Stereoscopic three-dimensional vision requires cortical processing for horizontal binocular disparity between the two eyes' retinal images. Behavioral and theoretical studies suggest that vertical size disparity is used to recover the viewing geometry and to generate the slant of a large surface. However, unlike horizontal disparity, the relation between stereopsis and neural responses to vertical disparity remains controversial. To determine the role of cortical processing for vertical size disparity in stereopsis, we measured neuromagnetic responses to disparities in people with good and poor stereopsis, using magnetoencephalography (MEG). Healthy adult participants viewed stereograms with a horizontal or vertical size disparity, and judged the perceived slant of the pattern. We assessed neural activity in response to disparities in the visual cortex and the phase locking of oscillatory responses including the alpha frequency range using MEG. For participants with good stereopsis, activity in the visual areas was significantly higher in response to vertical size disparity than to horizontal size disparity. The time–frequency analysis revealed that early neural responses to vertical size disparity were more phase-locked in good stereo participants than in poor stereo participants. These results provide neuromagnetic evidence that vertical-size disparity processing plays a role in good stereo vision.

1. Introduction

To perceive a stereoscopic three-dimensional (3-D) scene, the human brain must analyze horizontal binocular disparity between the two eyes' retinal images. The fine 3-D structure of a scene can be perceived from horizontal disparity, not from vertical disparity (Howard & Rogers, 2012). Many of, but not all of the general population (Bosten et al., 2015; Hess, To, Zhou, Wang, & Cooperstock, 2015) can see stereo depth from horizontal disparity (Richards, 1970). For subjects with good stereo vision, event-related potentials (ERPs) specific to horizontal disparity were found with a peak of ~250 ms relative to visual stimulus onset (Fahle, Quenzer, Braun, & Spang, 2003; Julesz, Kropfl, & Petrig, 1980; Spang, Gillam, & Fahle, 2012). For humans and monkeys with poor stereo vision, such ERP responses to horizontal disparity are absent or weak (Chao, Odom, & Karr, 1988; Janssen, Vogels, & Orban, 1999). Neuronal responses to horizontal disparity are likely to originate from multiple visual cortical areas that include the primary visual cortices (Hubel, Wiesel, Yeagle, Lafer-Sousa, & Conway, 2015; Neri, 2005; Sprague, Cooper, Tosic, & Banks, 2015). These visual areas include V1 (Prince, Cumming, & Parker, 2002), V2 (Hubel et al., 2015), V3, V3a (Backus, Fleet, Parker, & Heeger, 2001; Tsao et al., 2003), V4 (Brouwer, van Ee, & Schwarzbach, 2005; Durand, Peeters, Norman, Todd, & Orban, 2009), and the middle temporal (MT) area (Uka & DeAngelis, 2004; Joly, Vanduffel, & Orban, 2009).

In contrast to horizontal disparity, the relation between neural responses to vertical disparity and stereo vision remains controversial. One view is that the neural system does not necessarily encode non-zero vertical disparity (Cumming, 2002; Matthews et al., 2003). In line with this idea, Norcia, Gerhard, and Meredith (2017) and Avarvand et al. (2017) reported that ERP responses were weak for the stimulus that contained the vertical disparities that did not produce 3-D depth in human adults. The other contrasting view is that the neural system explicitly encodes vertical disparity (Mayhew & Longuet-Higgins, 1982; Serrano-Pedraza & Read, 2009) in order to achieve correct stereo correspondence and to produce a slant. Slant refers to a rotation of an object about an axis in the fronto-parallel plane and is distinguished from tilt, the orientation of the rotation axis (Banks, Hooge, & Backus, 2001). Although behavioral studies suggest the importance of vertical disparity in slant perception (Rogers & Bradshaw, 1993; Kaneko & Howard, 1996), the neural mechanisms that underlie vertical disparity

* Corresponding author.
E-mail address: hmitsudo@lit.kyushu-u.ac.jp (H. Mitsudo).

https://doi.org/10.1016/j.visres.2019.08.009
Received 4 February 2019; Received in revised form 15 August 2019; Accepted 21 August 2019
Available online 23 September 2019

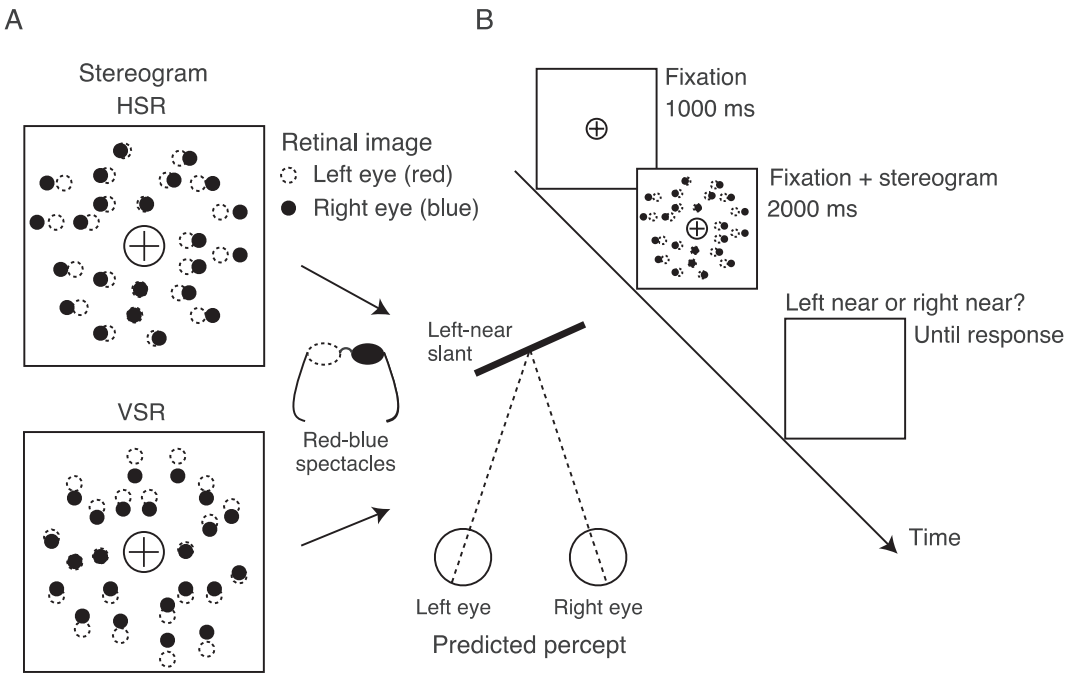

Fig. 1. Schematic illustration of the stimulus and trial sequence. A: Random-dot stereograms with horizontal or vertical size disparity (HSR or VSR, respectively) produce perceived slant about a vertical axis for good stereo observers. B: After a presentation of the fixation pattern (1 s), the random-dot stereogram was presented for 2 s. Subjects were asked to report which side of the stereo surface appeared in front of the fixation. Actual stimulus elements (dots and fixation pattern) were drawn against a dark backgroud. Illustrations are not drawn to scale.

encoding are largely unknown.

This study focuses on one specific type of vertical disparity that can be created by scaling or magnifying one eye's image of a binocularly viewed pattern in the vertical direction, called the vertical size ratio (VSR: Backus, Banks, van Ee, & Crowell, 1999). When VSR ≠ 1, the pattern contains a constant vertical gradient of local vertical disparities. In the interesting induced effect (Ogle, 1950), when viewing such stereograms (e.g., VSR = 1.05) in straight-ahead gaze, human observers can perceive a non-zero slant of the stimulus about a vertical axis. In a natural 3-D scene, the value of VSR is close to 1 around the fovea with straight-ahead gaze and systematically changes depending on the horizontal binocular gaze position and viewing distance. The VSR is distinguished from other types of disparity, such as the headcentric disparity defined by the binocular gaze position (Erkelens & van Ee, 1998), vertical shear disparity (Howard & Kaneko, 1994), and a horizontal gradient of vertical or horizontal disparity (Backus et al., 1999).

We hypothesized that the neural system of people with good stereopsis is particularly sensitive to the onset of stereograms with VSR. We adopted this hypothesis because our behavioral study (Mitsudo, Sakai, & Kaneko, 2013) suggested that VSR is used to first determine the geometry of the epipolar lines along which horizontal disparities are measured to produce the fine 3-D structure. Alternatively, induced neural responses to disparities, not necessarily locked to the stimulus onset, might be related to perception, given that 3-D slant can be perceived better at long stimulus presentations (van Ee & Erkelens, 1996; Harada & Mitsudo, 2018). The previous studies have not been conclusive on this issue.

In an attempt to explore the neural responses to vertical disparity, we used magnetoencephalography (MEG), which has better spatial resolution to distinctively evaluate the activated brain regions compared with electroencephalography. Unlike the stereograms used in the studies of Norcia et al. (2017) and Avarvand et al. (2017), we varied the amount of HSR and VSR. We presented random-dot stereograms simulating a 3-D slant at a fixed level of mean luminance to cancel out the effect of stimulus luminance on the evoked electromagnetic response components (Duan, Yakovleva, & Norcia, 2018). Our stereograms had HSR or VSR values that could produce a similar 3-D appearance of slant about a vertical axis. We used fixed values of HSR and VSR rather than adjusting them to individual observers, particularly because preliminary observations suggested that it was too difficult to obtain a reliable estimate of VSR threshold in a restricted viewing time for stereo-poor participants. While controlling the stimulus parameters, we tried to reveal the different neural processing for horizontal and vertical size disparity at the group level by comparing MEG responses to these stereograms in combination with individuals' behavioral sensitivity to the 3-D slant. In addition, since the mean luminance values of our HSR and VSR stereograms were matched, we assumed that their differences in MEG responses reflect disparity-based processing. In the first step of our analysis, the minimum-norm estimation technique (Hämäläinen & Ilmoniemi, 1994) was adopted to localize the MEG responses. Then, we assessed the time course of neuronal activity relative to stimulus onset in the visual cortex. Finally, we assessed the phase locking of alpha-band responses (8–14 Hz) (Hanslmayr et al., 2005; Palva, Linkenkaer-Hansen, Näätänen, & Palva, 2005) because the phase dynamics of electromagnetic responses around the time of stimulus onset in the alpha-band frequency are suggested to reflect sensory perception.

2. Materials and methods

2.1. Participants

Twenty-five healthy subjects participated in the experiment (age range, 20–26 years; 23 females; 23 right-handed). All subjects had normal or corrected-to-normal (by contact lenses) visual acuity and were naive as to the purpose of the experiment. The stereo fly test (Stereo Optical Co. Inc., Chicago, IL, USA) was performed before the experiment. Written consent was obtained from all participants. The experimental protocol was approved by the ethics committee at the Kyushu University Hospital (No. 27044). The experiment was carried out in accordance with the latest version of the Declaration of Helsinki.

2.2. Visual stimuli and procedure

Fig. 1 shows a schematic overview of the stimulus presentation and the experimental sequence. Visual stimuli were presented using a DLP projector (PG-F212X, Sharp Co. Ltd, Sakai, Japan) at a resolution of 1024 × 768 pixels at 60 Hz. The stimulus presentation was controlled by a laptop computer (Macbook Air, Apple Inc., Cupertino, CA, USA). To create anaglyph stereo stimuli with binocular disparity, blue and red stimulus elements were viewed through spectacles with blue and red filters in front of the right and left eyes, respectively. All stimulus elements were drawn with the antialiasing method. The interocular crosstalk was 7% on average and small enough to produce the desired disparity. The stereo stimulus consisted of ~750 dots presented in randomized positions within a circular region with a diameter of 31.6° of visual angle. The position of each dot was displaced according to given HSR and VSR values in order to prepare stereograms. Each dot was 6 × 6 pixels (without blur). After the VSR or HSR was introduced, the dots were finally blurred with a Gaussian kernel (a radius of 3.6 pixels). Because slant about a vertical axis is perceived better in the retinal periphery (Kaneko & Howard, 1996), the dots were presented outside a central circular region with a diameter of 7.5°. Peripheral objects in the subject's visual field (e.g., the edge of the MEG dewar) were almost invisible in the darkened room, so as to minimize the effect of surrounding frames on slant perception from VSR (van Ee & Erkelens, 1995). Fig. 1A represents horizontal and vertical size disparities that were introduced into the whole pattern, which are known to produce perceived slant about a vertical axis for good stereo observers (the geometrical and induced effects, respectively: (Ogle, 1950; Serrano-Pedraza & Read, 2009)). Since cortical MEG signals have a low signal-to-noise ratio, we needed to maximize the number of repetitions per condition. Therefore, we used two values for each of HSR and VSR conditions, so as to produce a moderate slant magnitude for stereo-normal observers in our slant-discrimination task. Because earlier studies suggested that perceived slant changed almost linearly in a VSR range of around 1/1.05–1.05, and declined outside this range (Ogle, 1950), we selected VSR values of 1/1.05 and 1.05 (the left eye's image size divided by the right eye's image size). According to Kaneko and Howard (1996), where the slant magnitude was compared between HSR and VSR for random-dot stimuli without respective cues as in this study, perceived slant from VSR was almost half that from HSR. In order to approximately match the slant magnitudes from HSR and VSR, we used size ratios of 1.025 and 1/1.025 in the HSR condition. The predicted slant magnitudes of the HSR and VSR conditions were 21° and 37° respectively with respect to the fronto-parallel plane (Backus et al., 1999, with an assumed interocular distance of 6.5 cm). The horizontal gaze angle predicted from the VSR value was ± 50° with respect to the mid-sagittal plane. A fixation pattern (a cross surrounded by a circle; 2.7° × 2.7° of visual angle) with vertical nonius lines was presented at the center of the screen. The maximal luminance levels of the red and blue stimuli were 13.4 and 5.2 cd/m^2, respectively; the mean background luminance levels were 0.08 cd/m^2 (through red-blue spectacles).

The subjects viewed the screen in the upright head position of the MEG dewar at a viewing distance of 102 cm. The experimental room was dark except for the stimulus. At the beginning of each trial, the fixation pattern against the dark background was presented for 1 s, followed by the sudden appearance of the random-dot stereogram (Fig. 1B). This type of presentation produces a salient luminance change at the time of stimulus onset, compared with an alternated presentation of similar stimuli with and without disparity (e.g., Norcia et al., 2017). The rationale for this presentation was to maximize disparity-specific evoked responses, which interact with responses to the monocular luminance-defined pattern (Duan et al., 2018). The random-dot pattern was presented for 2 s, followed by a blank display. The subjects were asked to report which side of the random-dot surface appeared in front of the fixation. They did this by a right- or left-button click after the disappearance of the stereogram. The subjects used the mouse with their right hand, and no speedy response was required. The left- and right-button clicks were made with the index and middle fingers, respectively. A mouse click triggered the next trial. The subjects were asked to fixate the center of the screen during the fixation mark or the stereo stimulus was presented. During this period, the subjects were also asked to suppress eye blinks as much as they could. In a run, 40 stimuli (2 disparity types × 2 slant orientations × 10 repetitions) were presented in a randomized order. Before the MEG measurement, each subject underwent at least two practice runs with feedback on response accuracy for each trial. In the practice runs, the response feedback was provided by a transient change (0.5 s) of the fixation mark to a negative sign for an incorrect response. In the MEG session, each subject completed five or six runs. The first run also served as practice, and thus the remaining runs were analyzed.

2.3. MEG recording

The experiment was conducted in a quiet, magnetically shielded room. Data were acquired by a 306-channel MEG system consisting of 204 planar gradiometers and 102 magnetometers (Neuromag, Elekta, Helsinki, Finland). MEG signals were continuously recorded at a sampling rate of 1000 Hz with a bandpass filter of 0.1–330 Hz. Before the MEG recording, four head position indicator (HPI) coils were attached to the subject's head. For each subject, the positions of three anatomical landmarks (nasion and left and right pre-auricular points) and the four HPI coils, and the individual head shape (at least 200 points) and stable positions of the forehead and nose (Hironaga et al., 2014) were measured with a 3-D digitizer (FASTRAK, Polhemus, VT, USA). Before each run, HPI measurement was performed. Trigger signals were set with respect to visual stimulus onset and a mouse click. The lag of visual stimulus onset relative to the trigger signal was measured by an oscilloscope (PDS6062T, Lilliput, Xiamen, China) before the experiment. The mean lag was 40 ms and corrected in data analysis. During the MEG measurement, the subjects were in the upright position, and head placement was adjusted so that the posterior part of the head touched the MEG dewar in a comfortable position. The subjects were also asked to minimize head and body movements, and the behavior of each subject was monitored during the MEG measurement.

2.4. MEG data analysis

In principle, MEG data provide temporal information in millisecond resolution. By applying a source localization technique to the data, we can obtain high-resolution signals from specific brain regions. We analyzed the time course and time–frequency components of these signals with phase locking metrics and additional statistics. Our MEG analyses consisted of pre-processing (Section 2.4), source localization (Section 2.5), time–frequency analysis (Section 2.6), and statistical tests (Section 2.7). All data sets were pre-processed using Maxfilter and Maxmove (Taulu, Kajola, & Simola, 2004; Taulu & Simola, 2006) to eliminate noise outside of the brain, to interpolate data from bad channels, and to spatially transform data into the default head position in the MEG dewar. The core parts of data analysis, signal processing, source localization, and statistical testing were performed with the Fieldtrip toolbox (Oostenveld, Fries, Maris, & Schoffelen, 2011) running on MATLAB software (version R2015, Mathworks, Natick, MA, USA). Our MEG analysis was performed generally along the guidelines proposed by Gross et al. (2013). Trials with excessive noise or flat signals were removed following visual inspection. Independent component analysis (ICA; the infomax algorithm: Bell & Sejnowski, 1995) was performed to remove artifacts of eye blinks, eye movements, and cardiac responses with visual inspections for ICA components.

For a source localization analysis, data were low-pass filtered at 50 Hz and then averaged across left-near and right-near slant trials and analyzed separately for each disparity condition (minimum n of

trials = 76). For the time–frequency analysis, we used data from all the 102 magnetometers, in an attempt to capture neural signals originating from the gyri or sulci of the cortex, whose magnetic responses are sometimes distant from neighboring sensor positions or originate from deeper locations inside the brain (Garcés, Lopez-Sanz, Maestu, & Pereda, 2017).

2.5. Source localization analysis

To investigate the source regions where neural activity occurs in response to disparities, we used the minimum-norm estimation technique (Hämäläinen & Ilmoniemi, 1994; Hashizume & Hironaga, 2016). In order to improve source localization accuracy, both data from the gradiometers and magnetometers were used for the source analysis. We used a standardized brain (MNI-305; Montreal Neurological Institute; Collins, Neelin, Peters, & Evans, 1994) and each subject's head shape obtained through a 3-D digitizer was used to co-register and construct the head models. For lead-field matrix computation, the realistic single-shell head model was used. For the source model, 8196 dipoles constrained by a cortical mesh were marked in the brain. A noise covariance matrix was created using data collapsed between the HSR and VSR conditions from −100 to 0 ms relative to stimulus onset. Noise-normalized source estimation (dynamic statistical parametric mapping; Dale et al., 2000) was performed in each disparity condition for −100 to 2000 ms. Estimated source activity was mapped onto a 3-D grid (left/right, posterior/anterior, and bottom/up axes: 18 cm × 21.6 cm × 18 cm; 1 voxel = 4 mm × 4 mm × 4 mm). For each disparity condition and subject, source activity was normalized by the value averaged over the whole brain for −100 to 0 ms, because estimated activity values differed considerably across cortical positions and subjects even for the baseline period. To tolerate individual differences in latency, source activity was temporally smoothed by a 25-ms averaging window, spatially smoothed by a Gaussian kernel (full-width half-maximum = 6 mm × 6 mm × 6 mm), and downsampled at 100 Hz. In addition to source activity, as an index of the activity difference between the HSR and VSR conditions, we calculated the ratio of activity in the VSR condition to that in the HSR condition at each voxel for each subject.

2.6. Time-frequency analysis

Event-related oscillatory phase and amplitude responses to disparities were analyzed by time–frequency decomposition for data from individual trials. The Fast-Fourier Transform algorithm was applied with a Hanning window of 0.5 s for every 2-Hz bin at center frequencies of 2–30 Hz. The window was shifted by every 50 ms from −0.5 to 2 s relative to the stimulus onset. To calculate the degree of phase locking relative to stimulus onset across trials, we calculated the phase locking factor (*PLF*; Tallon-Baudry, Bertrand, Delpuech, & Pernier, 1996; Delorme & Makeig, 2004) for each time across the trials,

$$PLF(t) = \left| \sum_{k} exp(i\varphi_k(t, f)) \right| / N \quad (1)$$

where i is the imaginary unit, and φ is the phase of each time–frequency component of MEG sensor signals obtained at its central frequency f from trial k ($k = [1, 2, \cdots, N]$) in each condition (no locking = 0; perfect locking = 1). The *PLF* is a measure of the stability of oscillatory neural activity across trials and is said to reflect long-range cortical connections (Voloh & Womelsdorf, 2016). The *PLF* values were analyzed and averaged for the alpha-band frequency range (8–14 Hz) because this range is predominantly related to sensory processes including vision (Hanslmayr et al., 2005; Buffalo, Fries, Landman, Buschman, & Desimone, 2011; Voloh & Womelsdorf, 2016).

To examine the relation between phase dynamics and stereo performance further, in addition to the *PLF*, we assessed the degree of phase shifts between two time points, the stimulus onset time (0 ms) and the target time at which phase locking was maximal. Supplementary Fig. S1 shows a summary of our phase shift analysis. The basic idea for the phase shift analysis is that, if phase locking at the target time accompanies successful coding for sensory input stimuli, slant-judgment performance will be improved when the phase angle in a trial comes closer to the angle of maximal phase locking. To obtain the metric of the phase shift, the phase angle θ_{PLF} corresponding to the obtained *PLF* value using Eq. (1) was subtracted from the phase angle in the kth trial at t ms, $\theta_{t,k}$ and the absolute value was calculated ($0 \leq |\theta_{t,k} - \theta_{PLF}| \leq \pi$). To calculate the baseline phase angle at $t = 0$ ms, the mean phase at the target time was shifted by $-2\pi ft$:

$$\theta_{PSbase} = \theta_{PLF} - 2\pi ft \quad (2)$$

Then, θ_{PSbase} was subtracted from the phase angle at the stimulus onset time $t = 0$ ms in each trial $\theta_{0,k}$, and the absolute value was calculated ($0 \leq |\theta_{0,k} - \theta_{PSbase}| \leq \pi$). Finally, the phase shift difference in the kth trial was obtained by:

$$PS_{diff} = |\theta_{t,k} - \theta_{PLF}| - |\theta_{0,k} - \theta_{PSbase}| \quad (3)$$

The values of PS_{diff} were negative in some trials (Supplementary Fig. S1A) and were close to zero in other trials (Supplementary Fig. S1B). PS_{diff} was calculated for each central frequency range of 8–14 Hz and for each of the 15 significant sensors at target time $t = 200$ ms, and then averaged for each subject. The target time was chosen because the maximal number of significant sensors was found in this period. For each disparity condition, single trials were categorized into two bins, based on the value of the mean phase shift difference (Eq. (3)), in order to calculate the sensitivity (d'; Macmillan & Creelman, 1991) to stereo slant. The sensitivity difference was calculated by subtracting the d_1' obtained from the trial bin where $PS_{diff} \geq M$ (labeled as smaller phase-shift trials) from the d_2' obtained from the other bin where $PS_{diff} < M$ (labeled as greater phase-shift trials), in which M represents the median value.

Power data from individual trials were averaged for each frequency range, disparity condition, and subject. Baseline correction was applied by subtracting log-transformed power values averaged over a pre-stimulus period from log-transformed power values for each bin. The baseline pre-stimulus period was −250 to −100 ms relative to stimulus onset, in order to minimize a temporal overlap between the baseline and post-stimulus periods.

2.7. Statistical analyses

To examine the relation between behavioral performance and neuronal responses to stereo stimuli, the subjects were divided into two groups. The criterion for grouping was their slant-judgment performance level in the HSR condition, because perceived depth from horizontal disparity is a widely used measure of stereo performance (e.g., stereo acuity: Chao et al., 1988; Oishi, Takemura, Aoki, Fujita, & Amano, 2018). We have not used the behavioral performance in the VSR condition for subject grouping because it is unknown how many of the population can see the induced effect, and it would make it difficult to compare previous reports and the present results. In this study, we regarded 0.75 as a boundary of stereo performance because this value is the midpoint between the chance level of 0.5 in our two-alternative forced-choice task and the upper performance limit of 1.0. Subjects whose correct response rate exceeded 0.75 were labeled as a good stereo group, and subjects whose correct response rate did not exceed 0.75 were labeled as a poor stereo group. We also used behavioral performance d' as a continuous variable in our additional analysis (see Sections 2.6 and 3.3).

We adopted a data-driven approach to finding differences in a subset of spatiotemporal MEG responses (sensor or voxel × time) between the HSR and VSR conditions and between the good and poor stereo subjects. We controlled an inflation of alpha level due to multiple

comparisons, by using two-step non-parametric cluster-based permutation tests (Maris & Oostenveld, 2007) on data from a relatively large region and time of interest (ROI and TOI, respectively). First, two-tailed *t* tests were performed for each sensor or voxel at each time point. Second, neighboring sensors or clusters with $p < 0.05$ were grouped into a larger cluster based on the spatiotemporal relationship, and used for a permutation-based test (resampling size = 1000). Two-tailed tests were performed for each permutation test. The *p* values from permutation tests are indicated by the label "corrected" in the Results section.

To examine evoked responses to disparities, the TOI was defined as 0–600 ms relative to the stimulus onset in the source localization analysis. To analyze temporal dynamics of the *PLF* and induced powers including a later period, the TOI was defined as 0–2000 ms in the time–frequency analysis. For the source localization analysis, because our primary concern was visual cortical processing, the visual ROI was defined as all the 25 atlas areas of the visual topographic probabilistic maps (VTPM; Wang, Mruczek, Arcaro, & Kastner, 2015). In additional statistical tests, ROIs were defined using brain atlas regions defined by the automated anatomical labeling (AAL; Tzourio-Mazoyer et al., 2002).

To examine whether the phase locking responses to VSR predicted stereo performance, we performed a multiple linear regression analysis. The three regression parameters were an intercept and two coefficients for the two *PLF*s for the HSR and VSR conditions obtained at 200 ms relative to stimulus onset for each subject (averaged across the alpha frequencies and the 15 significant sensors). The dependent variable was the behavioral sensitivity d' in the HSR condition calculated for each subject.

3. Results

3.1. Behavioral data

The stereo acuity measured with the stereo fly test varied across the subjects (circles stereo test: mean, 47 ± 21 (*SD*) arc sec of visual angle). None was stereo-blind because all were equal or above a stereo test disparity of 140 arc sec, which is not the lowest level of the stereo test patterns. The mean correct response rates for the slant-judgment task averaged over the 25 subjects were 0.78 for the HSR condition and 0.60 for the VSR condition. A significant positive correlation was found between the HSR and VSR conditions in correct response rates ($r = 0.67$, $p = 0.0002$, two-tailed). We also found a significant positive correlation between the correct response rate in the HSR condition and the stereo acuity ($r = 0.51$, $p = 0.01$, two-tailed), but not between the correct response rate in the VSR condition and stereo acuity ($r = 0.26$, $p = 0.21$, two-tailed).

According to the criterion stated in Section 2.7, the subjects were divided into the good ($n = 13$) and poor ($n = 12$) stereo groups. Visual inspections suggested that the correct response rates were distributed bimodally with respect to performance in the HSR condition (Fig. 2). This pattern is qualitatively consistent with the results of Hess et al. (2015) and somewhat different from those of Bosten et al. (2015), in that a single clear peak of the distribution was not found. Age was not significantly different between the two groups ($t(17.3) = 0.50$, $p = 0.62$, $d = 0.20$, two-tailed).

3.2. Enhanced source responses to vertical size disparity in the visual cortex

We examined whether visual cortical areas respond differently to horizontal and vertical size disparities, by calculating the location and strength of source activity for each subject. Source activity in the good stereo group was significantly higher in response to VSR than to HSR for 230–600 ms (cluster-based permutation test; $p = 0.014$, corrected). Fig. 3A represents the significant voxels revealed by the permutation test (mainly including visual areas V1, V2, and V3), with colors showing the durations at which enhanced activity was observed for

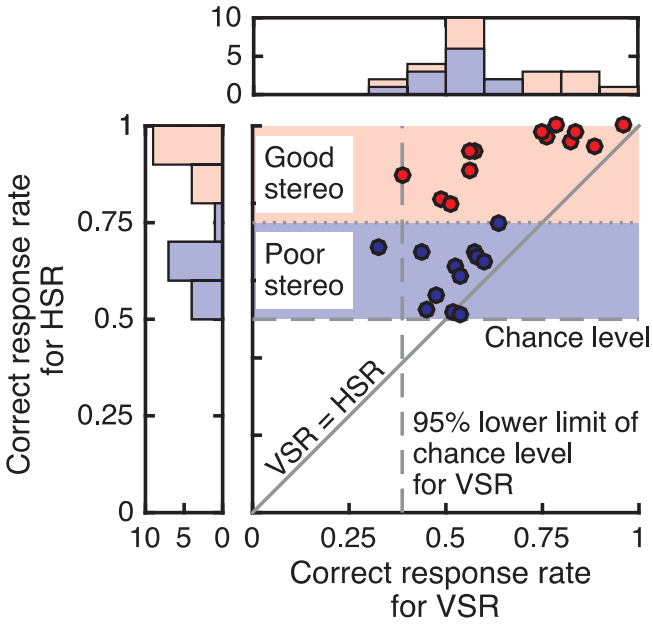

Fig. 2. Behaviral results for the slant-judgment task ($n = 25$). Scatter plots represent data from each subject. Twenty-five subjects were divided into good and poor stereo groups, based on a correct-response criterion level of 0.75 in the HSR condition. The leftmost and top histograms represent group differences in slant-judgment performance for the HSR and VSR conditions, respectively.

VSR. To check the reliability of our source analysis, we also performed a permutation test with a larger ROI of the AAL atlas that included most of the VTPM atlas. Even with the larger ROI, we also found a significant cluster where source activity was higher in response to VSR than to HSR for 200–600 ms in the good stereo group ($p = 0.036$, corrected). As an additional explanatory analysis, we further split the good stereo group into two subgroups, using the criterion of the correct response rate ≥ and < 0.75 in the VSR condition (*n*s = 7 and 6, respectively). Consequently, no significant difference in source activity was found between the HSR and VSR conditions in either of the good stereo subgroups (*p*s ≥ 0.08, corrected). Since many previous EEG studies showed that evoked neural responses become stronger in general as perceived depth (or stimulus disparity) increases up to a certain limit (Chao et al., 1988; Norcia et al., 2017; Avarvand et al., 2017), the perceived slant magnitude (HSR > VSR) is unlikely to explain enhanced responses to VSR.

In contrast to the good stereo group, no statistically reliable clusters were found where activity differed between the two disparity conditions in the poor stereo group (*p*s = 1). Since the magnitude of disparity was greater for VSR than for HSR, the disparity magnitude is not the sole factor that determines neural responses for each stereo group. The vertical/horizontal activity ratio significantly differed between the good and poor stereo groups for 240–480 ms ($p = 0.04$, corrected), suggesting an interaction between disparity type and stereo group.

Since Fig. 3A shows the enhanced activity in response to VSR particularly in V1d, we calculated the time course of averaged source activity over V1d. The top panel of Fig. 3B represents the results for the good stereo group, showing the enhanced source activity in response to VSR for 230–600 ms found in the cluster-based test (indicated by the gray shaded area). The onset timing of the difference between the two disparity conditions is consistent with that of disparity-specific ERP responses at ~ 250 ms relative to stimulus onset (Fahle et al., 2003; Spang et al., 2012). For the results of the poor stereo group shown in the bottom panel of Fig. 3B, the time course of source activity was very similar between the two disparity conditions. Compared with the top panel of Fig. 3B, the overall activity level was close to or less than that of the HSR condition in the good stereo group. These results can be

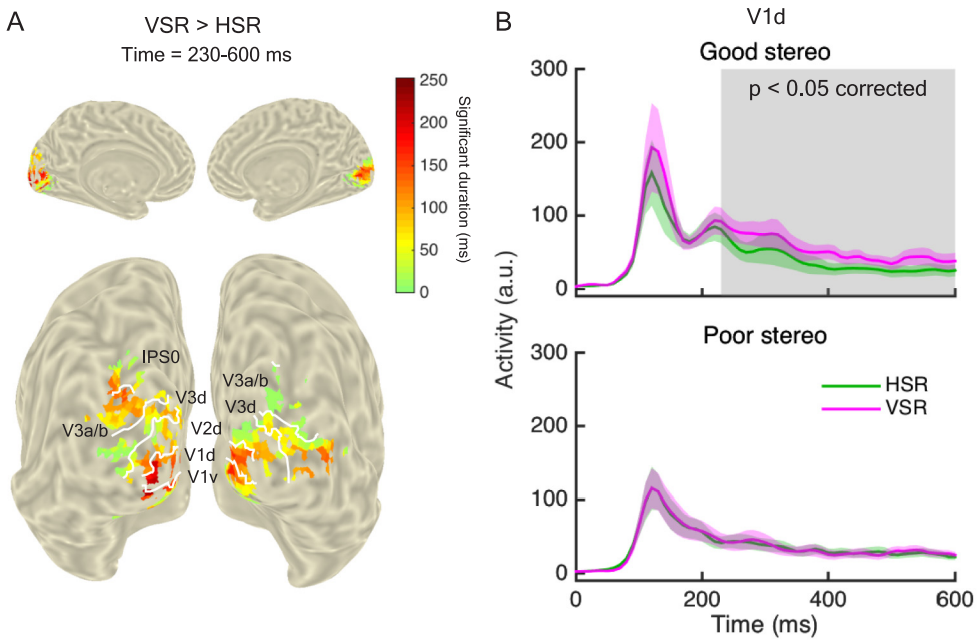

Fig. 3. Enhanced source activity to VSR over HSR in the visual cortex of the good stereo subjects. A: Significant voxels mapped onto left and right inflated cortical surface models ($p < 0.05$, corrected). Colors represent cumulative durations for which enhanced activity was found within 230–600 ms relative to the stimulus onset. The top panel shows two medial views, while the bottom panel shows an occipital view. B: The comparison of V1d activities (standardized dSPM values) in the two disparity conditions, HSR (green) vs. VSR (magenta) for the good stereo group (top) and the poor stereo group (bottom). Time course of group-averaged V1d activity is consistent with the enhanced responses to VSR in the good stereo group (gray shaded area). Color-shaded areas in B represent the standard errors of the mean (SEMs). (For interpretation of the references to color in this figure legend, the reader is referred to the web version of this article.)

interpreted as indicating the near absence of neural responses associated with the direction of size disparity in the poor stereo group. This is analogous to the absence of disparity-specific ERP responses in stereo-anomalous subjects (Chao et al., 1988). We also analyzed event-related field (ERF) responses to disparities between two groups at sensor level, and found no statistically reliable differences between the disparity conditions or between the groups (see Supplementary Results and Fig. S2). In sum, we found that the visual source activity of good stereo subjects was enhanced in response to VSR for 230–600 ms relative to the stimulus onset.

3.3. Phase locking to vertical size disparity

Since the source localization analysis revealed that the good stereo subjects showed enhanced source activities in response to VSR (Fig. 3), we further calculated *PLF*s for alpha-band responses to assess the degree of phase resetting to VSR around the stimulus onset. Fig. 4A shows group-averaged comparisons between the alpha-band phase locking in the good stereo group and that in the poor stereo group for each disparity condition. The top panel of Fig. 4A shows that, in the HSR condition, no clusters were found where *PLF*s were significantly different between the two groups ($p = 0.080$, corrected). The bottom panel of Fig. 4A shows that, in the VSR condition, *PLF*s were significantly greater in the good stereo group than in the poor stereo group for 0–300 ms in the left occipital, parietal, and temporal sensors (Fig. 4B; the maximal n of sensors was 15 at 200 ms; $p = 0.038$, corrected). Since the stimulus disparity was constant in this group-level comparison, the disparity magnitude does not explain the PLF differences between the good and poor stereo groups.

To examine whether the phase locking responses to VSR at 200 ms predict individual behavioral performance in the HSR condition, we performed a multiple linear regression analysis. The three-parameter regression model was statistically significant ($df = 22$, $p = 0.0044$, adjusted $R^2 = 0.33$). The partial regression coefficient was significantly greater than 0 for VSR (partial regression coefficient = 21.1; $p = 0.027$) but not for HSR ($p = 0.21$). For the purpose of visualization, Fig. 4C shows a positive correlation between the *PLF* for VSR and behavioral sensitivity to HSR. We also performed a similar multiple linear regression analysis on the behavioral sensitivity in the VSR condition, and found that the regression was not significant ($df = 22$, $p = 0.086$, adjusted $R^2 = 0.13$). Taken together, the results of our multiple linear regression analysis showed that phase locking responses to VSR, rather than to HSR play a key role in predicting behavioral performance for HSR across good and poor stereo subjects.

After establishing the relationship between the early alpha-band phase locking to VSR stereograms and behavioral performance at the group level, we also analyzed phase data from single trials (see Supplementary Fig. S1). We calculated sensitivity (d') differences on slant judgment between two trial bins in which the phase shift was smaller and greater. Fig. 4D shows that the phase-shift-related d' change for the VSR condition was positively correlated with the individual's *PLF* value for the good and poor stereo groups ($r = 0.45$; $p = 0.025$). This implies that in trials where the phase angle became closer to the angle of maximal phase locking, stereo performance in the VSR condition improved in subjects showing a higher degree of phase locking. In the HSR condition, the d' change was not correlated with *PLF* ($r = 0.04$; $p = 0.85$). These analyses support the idea that phase-locked neural responses to VSR are related to good behavioral performance.

We also examined whether the power of alpha-band responses differed between conditions and between subjects. Fig. 4E and F show a general decrease of the alpha-band power after stimulus onset, consistent with earlier studies (Palva et al., 2005; Amano et al., 2012). In the good stereo group (Fig. 4E), we found a marginally significant cluster where the decrease in alpha-band powers was smaller in response to HSR than to VSR for 1250–2000 ms in the right parietal sensors (the maximal n of sensors was 17 at 1850 ms; $p = 0.082$, corrected). In the poor stereo group, no significant cluster was found where the power of alpha-band responses was different between the two

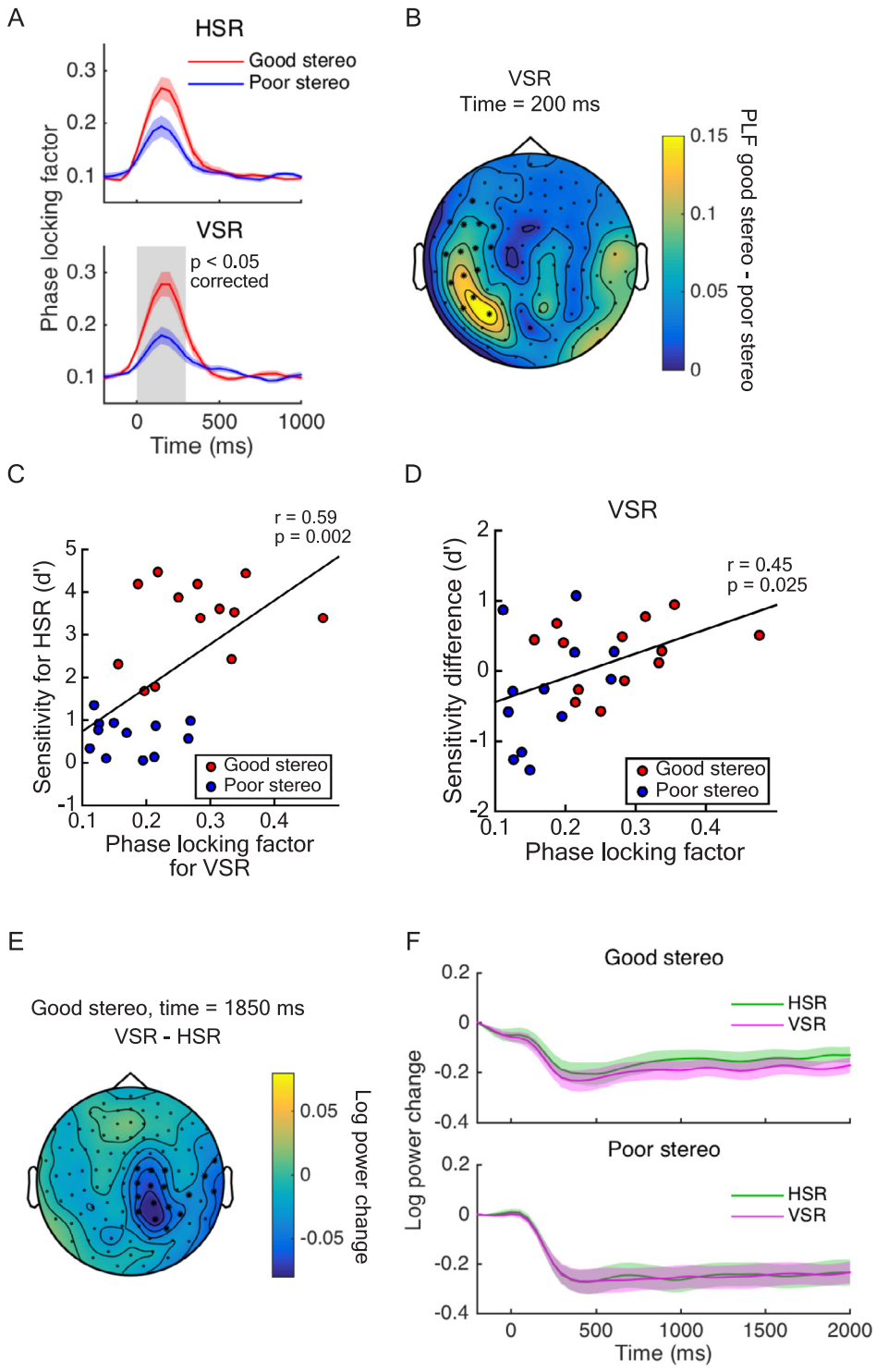

Fig. 4. Alpha-band (8–14 Hz) phase locking responses to VSR associated with good stereo performance. A: Group-averaged *PLF*s to VSR (bottom) but not to HSR (top) were significantly greater in the good stereo group than in the poor stereo group for 0–300 ms relative to the stimulus onset (gray shaded area; $p < 0.05$, corrected). *PLF*s were averaged across the asterisked sensors in B. Color-shaded areas represent SEMs. B: Differences in the topographic map of group-averaged *PLF*s between the good stereo and poor stereo groups. C: Inter-subject positive correlation between the *PLF* for VSR and behavioral sensitivity d' to HSR. *PLF* values were averaged across the asterisked sensors in B at 200 ms after the stimulus onset. D: The behavioral stereo sensitivity d' to VSR was associated with phase shifts relative to the angle of maximal phase locking within individual subjects. Phase shifts were calculated at 0 and 200 ms after stimulus onset for the asterisked sensors shown in B. E: The mean difference in log-transformed alpha-band power between the two disparity conditions (VSR - HSR) in the good stereo group at 1850 ms relative to stimulus onset. Asterisks indicate sensors in the largest cluster (but the cluster did not survive a permutation test). F: Comparison of mean power values averaged over the asterisked sensors in Panel E as a function of time relative to stimulus onset. Following the source localization analysis, powers were compared between the HSR (green) and VSR (magenta) conditions separately for the good stereo group (top) and the poor stereo group (bottom). Color-shaded areas represent SEMs. (For interpretation of the references to color in this figure legend, the reader is referred to the web version of this article.)

disparity conditions ($ps = 1$, corrected). We also did not find a significant cluster of sensors where alpha-band powers were different between the two groups in each disparity condition ($ps > 0.29$). These results suggest that alpha-band induced powers are not directly related to VSR processing.

4. Discussion

We found that activities in the early visual areas (V1-3) were significantly higher in response to VSR than to HSR for the good stereo subjects but not for the poor stereo subjects. The time–frequency analysis revealed that early neural responses to VSR in the alpha frequency range were more phase-locked in the good stereo subjects than in the poor stereo subjects. Overall, the present data support the idea that in people with good stereo vision, the neural visual system processes vertical size disparity as well as horizontal size disparity.

4.1. Comparison with previous studies

The results of our source localization analysis (Fig. 3) extend earlier

fMRI findings that multiple primary visual areas respond to horizontal disparity (Backus et al., 2001; Tsao et al., 2003), in that some of the early visual areas (V1-3) are also involved in VSR processing. The present results partly support the results of Arnoldussen, Goossens, and van Den Berg's (2015) fMRI finding that V1 is involved in VSR processing when retinal motion and vergence eye-movement signals are present. Furthermore, considering that mean perceptual discrimination performance for VSR-defined slant did not exceed that for HSR-defined slant in this study, the present MEG results are consistent with the results of Brouwer et al.'s (2005) fMRI results showing that *perceived* stereo slant is related to activity in V4d rather than in V1-3. The time–frequency analysis revealed that alpha-band oscillatory responses to VSR were more phase-locked in good stereo subjects than in poor stereo subjects at ~200 ms after the stimulus onset (Fig. 4). Previous ERP studies have suggested that (a) some evoked components (N170 and N270) are related to stereoscopic perception from horizontal disparity (Fahle et al., 2003; Spang et al., 2012), and (b) the exogenous N170 component is affected by the vertical gradient of horizontal disparity (Li, Jia, Chung-Fat-Yim, Jin, & Yu, 2017). The present results imply that the early ERP components may partly result from a phase resetting to the onset of stereograms, because we also observed phase locking to a certain degree in the HSR condition (i.e., zero vertical gradient of vertical disparity) in addition to the VSR condition (i.e., a non-zero vertical gradient of vertical disparity) at a similar range of 0–300 ms, particularly for good stereo subjects (Fig. 4A). Our source localization results also demonstrate that exogenous neural responses to VSR last up to ~600 ms relative to stimulus onset particularly at the visual cortex of good stereo subjects.

The primary contribution of this study is to demonstrate neural responses to VSR in people with good stereo vision. Chowdhury, Christiansen, Morgan, and DeAngelis (2008) recorded LFP responses from MT neurons in macaque monkeys viewing stereograms with VSR, and found that MT neurons are *not* sensitive to a change in VSR. Because Chowdhury et al. (2008) obtained reliable behavioral responses to VSR, they asserted that VSR is coded in regions other than MT. The present MEG study supports this view because our source analysis suggested that V1-3, but not hMT or MST respond more strongly to VSR than to HSR (the bottom panel of Fig. 3A). The present data generally support the view that stereopsis is achieved by cortical interactions between early visual areas including V1-3 (Sprague et al., 2015).

The enhanced early neuronal responses to VSR revealed by the present MEG study might be surprising, given that Norcia et al. (2017) and Avarvand et al. (2017) reported that ERP responses of human adult subjects were weaker when vertical disparity was added to the stimulus. What caused the discrepant results? The choice of the stimulus is a likely candidate because this study differed from the two previous studies mainly in terms of the type of vertical disparity. Given that disparity-related ERP responses primarily reflect stereoscopic depth processing, the mature adult brain may respond poorly to the vertical disparity that did not produce 3-D depth in the previous studies. In contrast, the stereogram used in this study contained a constant value of VSR across a large portion of the visual field and is in theory capable of producing an unambiguous percept predicted from the eccentric viewing geometry (Backus et al., 1999). The present and earlier studies indicate that neural responses to vertical disparity may differ depending on the spatial disparity structure.

4.2. Neural mechanisms underlying good stereo vision

Our source localization analysis suggests that enhanced activity in response to VSR in the visual areas begins at 200 ms after the stimulus onset (Fig. 3B). As proposed by Backus et al. (1999), a non-zero vertical size disparity (i.e., a constant value of VSR ≠ 1 across the entire visual field) may imply a horizontally averted gaze position in natural 3-D scenes, where the epipolar geometry changes across retinal positions. In this case, cortical computational resources may be required to somehow adjust the epipolar geometry compared with the case of VSR = 1, where "default" retina-fixed epipolar lines are available in straight-ahead gaze (van Ee & van Dam, 2003; Mitsudo, 2007). We speculate that such a computation for adjusting the epipolar geometry may accompany enhanced neural responses in the VSR condition for people with good stereo vision. This view is strengthened by the results obtained in the poor stereo group (the bottom panel of Fig. 3B), where no differences were found between the HSR and VSR conditions in the visual areas.

Higher alpha-band phase locking to VSR was found in subjects with good stereo vision (Fig. 4A–C), and slant-judgment performance for VSR was higher in trials where phase was closer to the angle of maximal phase locking, particularly for subjects showing a higher *PLF* (Fig. 4D). These between-subject and within-subject phase analyses suggest that good stereo vision may be partly achieved by neural mechanisms initiated by the alpha-band phase resetting to the onset of vertical size disparity. According to this idea, a higher degree of phase resetting occurs around at 200 ms (Fig. 4B) because VSR is presented across a relatively large visual field (~30° of visual angle), which requires alpha-band long-range oscillations within and across the visual areas (Frauscher et al., 2018) to code this information.

4.3. Relationships among stimulus features, task difficulty, and neural activity

An alternative interpretation of the present results is that enhanced responses to VSR in the good stereo group are due to (a) the magnitude of stimulus disparity we selected or (b) the magnitude of perceived slant. First, in our experiment, we selected a greater magnitude of size disparity in the VSR condition than in the HSR condition. According to EEG studies (Chao et al., 1988; Norcia et al., 2017), evoked neural responses increase as disparity magnitude increases. If evoked responses are determined by the disparity magnitude, MEG responses would be identical at the group level when disparity magnitudes were equated. However, this prediction was not supported by the phase locking analysis, because *PLF*s were greater for the good stereo group than for the poor stereo group in the VSR condition (Fig. 4A). Second, behavioral slant-discrimination performance was better for HSR on average (Fig. 2), suggesting that perceived slant magnitude would be greater for HSR than for VSR. According to Brouwer et al. (2005), neural responses increase as the magnitude of perceived depth increases. If this is the case, neural responses would be enhanced in the HSR condition. However, this prediction was not supported in the source localization analysis in either the good or poor stereo group. Therefore, neither the magnitude of stimulus disparity nor that of perceived slant accounts for all results.

Another possible explanation of the present results is a motivational difference between the good and poor stereo groups. The subjects in the poor stereo group might have been less motivated to perform the slant-judgment task than the subjects in the good stereo group, because the subjects in the poor stereo group may have been aware of their own low performance (e.g., from visual feedback on response accuracy during practice trials). This type of motivational difference might affect neuronal responses to disparities, whereby reward or attentional mechanisms modulate visual cortical processing (Apitz & Bunzeck, 2012; Lobier, Palva, & Palva, 2018). We believe that a motivational difference between the subject groups does not explain the present data, because we found a significant interaction effect between disparity type and stereo performance in the source localization analysis.

4.4. Limitations

Why did individuals' behavioral sensitivity differ considerably in the VSR condition as well as in the HSR condition? There are three possible reasons. First, individuals' vertical binocular fusion limit (Schor, Wood, & Ogawa, 1984) may not be perfectly correlated with the

horizontal fusion limit. Second, individuals' ability to spatially integrate or pool vertical disparity signals across a large portion of the visual field may be somewhat independent from their ability to extract and use horizontal disparity signals. These factors might contribute to their ability to correct the binocular epipolar geometry (Mitsudo, Kaneko, & Nishida, 2009; Mitsudo et al., 2013). Third, individual differences in the VSR condition may reflect the ability to integrate retinal VSR signals and extraretinal signals for gaze position (Backus et al., 1999). In this case, individuals who performed well in the VSR condition might be able to use VSR signals independently of the corresponding horizontal eye position (i.e., even in straight-ahead gaze in our case). To examine these possibilities, further studies will be necessary.

We compared neural responses between the HSR and VSR conditions where the stimuli differed in both the direction and the magnitude of size disparity. As discussed in Section 4.3, the enhanced responses in the VSR condition seem to be due to the direction of disparity. Nevertheless, it is still not clear the extent to which the magnitude of size disparity affects MEG responses to disparities. To examine this issue experimentally, it will be helpful to use stimuli with several magnitudes of HSR and VSR in future (including a zero disparity condition, i.e., HSR = VSR = 1).

4.5. Conclusions

We demonstrated that visual source activity was enhanced in response to vertical size disparity in people with good stereo vision. We also showed that alpha-band phase locking to vertical size disparity was related to stereoscopic slant judgment. Taken together, our study provides the first neuromagnetic evidence that vertical-size disparity processing plays a role in generating 3-D slant perception.

Declaration of Competing Interest

The authors declare that they have no known competing financial interests or personal relationships that could have appeared to influence the work reported in this paper.

Acknowledgements

We thank Shinya Harada, Emi Hasuo, Daiichiro Kuroki, Takako Mitsudo, Hisato Nakazono, and Akinori Takeda for their help and technical assistance in preparing the experiment. We are also grateful to the three anonymous reviewers for their helpful comments on an earlier version of this manuscript. This study was supported in part by JSPS KAKENHI Grant Numbers JP15K17327 and JP18K03180.

Appendix A. Supplementary data

Supplementary data to this article can be found online at https://doi.org/10.1016/j.visres.2019.08.009.

References

Amano, K., Takeda, T., Haji, T., Terao, M., Maruya, K., Matsumoto, K., ... Nishida, S. (2012). Human neural responses involved in spatial pooling of locally ambiguous motion signals. *Journal of Neurophysiology, 107*(12), 3493–3508. https://doi.org/10.1152/jn.00821.2011.

Apitz, T., & Bunzeck, N. (2012). Reward modulates the neural dynamics of early visual category processing. *Neuroimage, 63*(3), 1614–1622. https://doi.org/10.1016/j.neuroimage.2012.08.046.

Arnoldussen, D. M., Goossens, J., & van Den Berg, A. V. (2015). Dissociation of retinal and headcentric disparity signals in dorsal human cortex. *Frontiers in Systems Neuroscience, 9*, 16.

Avarvand, F. S., Bosse, S., Muller, K. R., Schafer, R., Nolte, G., Wiegand, T., ... Samek, W. (2017). Objective quality assessment of stereoscopic images with vertical disparity using EEG. *Journal of Neural Engineering, 14*(4), https://doi.org/10.1088/1741-2552/aa6d8b.

Backus, B. T., Banks, M. S., van Ee, R., & Crowell, J. A. (1999). Horizontal and vertical disparity, eye position, and stereoscopic slant perception. *Vision Research, 39*(6), 1143–1170.

Backus, B. T., Fleet, D. J., Parker, A. J., & Heeger, D. J. (2001). Human cortical activity correlates with stereoscopic depth perception. *Journal of Neurophysiology, 86*(4), 2054–2068. https://doi.org/10.1152/jn.2001.86.4.2054.

Banks, M. S., Hooge, I. T. C., & Backus, B. T. (2001). Perceiving slant about a horizontal axis from stereopsis. *Journal of Vision, 1*, 55–79. https://doi.org/10.1167/1.2.1.

Bell, A. J., & Sejnowski, T. J. (1995). An information-maximization approach to blind separation and blind deconvolution. *Neural Computation, 7*(6), 1129–1159.

Bosten, J. M., Goodbourn, P. T., Lawrance-Owen, A. J., Bargary, G., Hogg, R. E., & Mollon, J. D. (2015). A population study of binocular function. *Vision Research, 110*(Pt A), 34–50. https://doi.org/10.1016/j.visres.2015.02.017.

Brouwer, G. J., van Ee, R., & Schwarzbach, J. (2005). Activation in visual cortex correlates with the awareness of stereoscopic depth. *Journal of Neuroscience, 25*(45), 10403–10413.

Buffalo, E. A., Fries, P., Landman, R., Buschman, T. J., & Desimone, R. (2011). Laminar differences in gamma and alpha coherence in the ventral stream. *Proc. Natl. Acad. Sci. U.S.A. 108*(27), 11262–11267. https://doi.org/10.1073/pnas.1011284108.

Chao, G. M., Odom, J. V., & Karr, D. (1988). Dynamic stereoacuity: A comparison of electrophysiological and psychophysical responses in normal and stereoblind observers. *Documenta Ophthalmologica, 70*(1), 45–58.

Chowdhury, S. A., Christiansen, D. L., Morgan, M. L., & DeAngelis, G. C. (2008). Effect of vertical disparities on depth representation in macaque monkeys: MT physiology and behavior. *Journal of Neurophysiology, 99*(2), 876–887. https://doi.org/10.1152/jn.00732.2007.

Collins, D. L., Neelin, P., Peters, T. M., & Evans, A. C. (1994). Automatic 3D intersubject registration of MR volumetric data in standardized Talairach space. *Journal of Computer Assisted Tomography, 18*(2), 192–205.

Cumming, B. G. (2002). An unexpected specialization for horizontal disparity in primate primary visual cortex. *Nature, 418*(6898), 633–636.

Dale, A. M., Liu, A. K., Fischl, B. R., Buckner, R. L., Belliveau, J. W., Lewine, J. D., & Halgren, E. (2000). Dynamic statistical parametric mapping: Combining fMRI and MEG for high-resolution imaging of cortical activity. *Neuron, 26*(1), 55–67.

Delorme, A., & Makeig, S. (2004). EEGLAB: An open source toolbox for analysis of single-trial EEG dynamics including independent component analysis. *Journal of Neuroscience Methods, 134*(1), 9–21. https://doi.org/10.1016/j.jneumeth.2003.10.009.

Duan, Y., Yakovleva, A., & Norcia, A. M. (2018). Determinants of neural responses to disparity in natural scenes. *Journal of Vision, 18*(3), 21. https://doi.org/10.1167/18.3.21.

Durand, J. B., Peeters, R., Norman, J. F., Todd, J. T., & Orban, G. A. (2009). Parietal regions processing visual 3D shape extracted from disparity. *Neuroimage, 46*(4), 1114–1126. https://doi.org/10.1016/j.neuroimage.2009.03.023.

Erkelens, C. J., & van Ee, R. (1998). A computational model of depth perception based on headcentric disparity. *Vision Research, 38*(19), 2999–3018.

Fahle, M., Quenzer, T., Braun, C., & Spang, K. (2003). Feature-specific electrophysiological correlates of texture segregation. *Vision Research, 43*(1), 7–19.

Frauscher, B., von Ellenrieder, N., Zelmann, R., Dolezalova, I., Minotti, L., Olivier, A., ... Gotman, J. (2018). Atlas of the normal intracranial electroencephalogram: Neurophysiological awake activity in different cortical areas. *Brain, 141*(4), 1130–1144. https://doi.org/10.1093/brain/awy035.

Garcés, P., Lopez-Sanz, D., Maestu, F., & Pereda, E. (2017). Choice of magnetometers and gradiometers after signal space separation. *Sensors (Basel), 17*(12), https://doi.org/10.3390/s17122926.

Gross, J., Baillet, S., Barnes, G. R., Henson, R. N., Hillebrand, A., Jensen, O., ... Schoffelen, J. M. (2013). Good practice for conducting and reporting MEG research. *Neuroimage, 65*, 349–363. https://doi.org/10.1016/j.neuroimage.2012.10.001.

Hämäläinen, M. S., & Ilmoniemi, R. J. (1994). Interpreting magnetic fields of the brain: Minimum norm estimates. *Medical and Biological Engineering and Computing, 32*(1), 35–42.

Hanslmayr, S., Klimesch, W., Sauseng, P., Gruber, W., Doppelmayr, M., Freunberger, R., & Pecherstorfer, T. (2005). Visual discrimination performance is related to decreased alpha amplitude but increased phase locking. *Neuroscience Letters, 375*(1), 64–68. https://doi.org/10.1016/j.neulet.2004.10.092.

Harada, S., & Mitsudo, H. (2018). Stereoscopic slant contrast and the perception of inducer slant at brief stimulus presentations. *Perception, 47*(2), 171–184. https://doi.org/10.1177/0301006617739755.

Hashizume, A., & Hironaga, N. (2016). Principles of magnetoencephalography. In S. Tobimatsu, & R. Kakigi (Eds.). *Clinical Applications of Magnetoencephalography* (pp. 3–32). Tokyo: Springer doi: 10.1007/978-4-431-55729-6_1.

Hess, R. F., To, L., Zhou, J., Wang, G., & Cooperstock, J. R. (2015). Stereo vision: The haves and have-nots. *i-Perception, 6*(3), 1–5. https://doi.org/10.1177/2041669515593028.

Hironaga, N., Hagiwara, K., Ogata, K., Hayamizu, M., Urakawa, T., & Tobimatsu, S. (2014). Proposal for a new MEG-MRI co-registration: A 3D laser scanner system. *Clinical Neurophysiology, 125*(12), 2404–2412. https://doi.org/10.1016/j.clinph.2014.03.029.

Howard, I. P., & Kaneko, H. (1994). Relative shear disparities and the perception of surface inclination. *Vision Research, 34*(19), 2505–2517.

Howard, I. P., & Rogers, B. J. (2012). *Perceiving in Depth (Vol. 2). Stereoscopic Vision.* New York, NY: Oxford University Press.

Hubel, D. H., Wiesel, T. N., Yeagle, E. M., Lafer-Sousa, R., & Conway, B. R. (2015). Binocular stereoscopy in visual areas V-2, V-3, and V-3A of the macaque monkey. *Cerebral Cortex, 25*(4), 959–971. https://doi.org/10.1093/cercor/bht288.

Janssen, P., Vogels, R., & Orban, G. A. (1999). Assessment of stereopsis in rhesus monkeys using visual evoked potentials. *Documenta Ophthalmologica, 95*, 247–255.

Joly, O., Vanduffel, W., & Orban, G. A. (2009). The monkey ventral premotor cortex

processes 3D shape from disparity. *Neuroimage, 47*(1), 262–272. https://doi.org/10.1016/j.neuroimage.2009.04.043.
Julesz, B., Kropfl, W., & Petrig, B. (1980). Large evoked potentials to dynamic random-dot correlograms and stereograms permit quick determination of stereopsis. *Proc. Natl. Acad. Sci. U.S.A. 77*(4), 2348–2351.
Kaneko, H., & Howard, I. P. (1996). Relative size disparities and the perception of surface slant. *Vision Research, 36*(13), 1919–1930.
Li, H., Jia, H., Chung-Fat-Yim, A., Jin, L., & Yu, D. (2017). The neural correlates of vertical disparity gradient and cue conflict in Panum's limiting case. *Brain and Cognition, 114*, 11–19. https://doi.org/10.1016/j.bandc.2017.02.005.
Lobier, M., Palva, J. M., & Palva, S. (2018). High-alpha band synchronization across frontal, parietal and visual cortex mediates behavioral and neuronal effects of visuospatial attention. *Neuroimage, 165*, 222–237. https://doi.org/10.1016/j.neuroimage.2017.10.044.
Macmillan, N. A., & Creelman, C. D. (1991). *Detection Theory: A User's Guide.* Cambridge: Cambridge University Press.
Maris, E., & Oostenveld, R. (2007). Nonparametric statistical testing of EEG- and MEG-data. *Journal of Neuroscience Methods, 164*(1), 177–190. https://doi.org/10.1016/j.jneumeth.2007.03.024.
Matthews, N., Meng, X., Xu, P., & Qian, N. (2003). A physiological theory of depth perception from vertical disparity. *Vision Research, 43*(1), 85–99.
Mayhew, J. E., & Longuet-Higgins, H. C. (1982). A computational model of binocular depth perception. *Nature, 297*(5865), 376–378.
Mitsudo, H. (2007). Illusory depth induced by binocular torsional misalignment. *Vision Research, 47*(10), 1303–1314.
Mitsudo, H., Kaneko, H., & Nishida, S. (2009). Perceived depth of curved lines in the presence of cyclovergence. *Vision Research, 49*(3), 348–361. https://doi.org/10.1016/j.visres.2008.11.004.
Mitsudo, H., Sakai, A., & Kaneko, H. (2013). Vertical size disparity and the correction of stereo correspondence. *Perception, 42*(4), 385–400. https://doi.org/10.1068/p7387.
Neri, P. (2005). A stereoscopic look at visual cortex. *Journal of Neurophysiology, 93*(4), 1823–1826. https://doi.org/10.1152/jn.01068.2004.
Norcia, A. M., Gerhard, H. E., & Meredith, W. J. (2017). Development of relative disparity sensitivity in human visual cortex. *Journal of Neuroscience, 37*(23), 5608–5619. https://doi.org/10.1523/JNEUROSCI.3570-16.2017.
Ogle, K. N. (1950). *Researches in Binocular Vision.* Philadelphia, PA: W.B. Saunders.
Oishi, H., Takemura, H., Aoki, S. C., Fujita, I., & Amano, K. (2018). Microstructural properties of the vertical occipital fasciculus explain the variability in human stereoacuity. *Proc. Natl. Acad. Sci. U.S.A. 115*(48), 12289–12294.
Oostenveld, R., Fries, P., Maris, E., & Schoffelen, J. M. (2011). FieldTrip: Open source software for advanced analysis of MEG, EEG, and invasive electrophysiological data. *Computational Intelligence and Neuroscience, 2011*. https://doi.org/10.1155/2011/156869.
Palva, S., Linkenkaer-Hansen, K., Näätänen, R., & Palva, J. M. (2005). Early neural correlates of conscious somatosensory perception. *Journal of Neuroscience, 25*(21), 5248–5258. https://doi.org/10.1523/JNEUROSCI.0141-05.2005.
Prince, S. J., Cumming, B. G., & Parker, A. J. (2002). Range and mechanism of encoding of horizontal disparity in macaque V1. *Journal of Neurophysiology, 87*(1), 209–221. https://doi.org/10.1152/jn.00466.2000.
Richards, W. (1970). Stereopsis and stereoblindness. *Experimental Brain Research, 10*(4), 380–388.
Rogers, B. J., & Bradshaw, M. F. (1993). Vertical disparities, differential perspective and binocular stereopsis. *Nature, 361*(6409), 253–255. https://doi.org/10.1038/361253a0.
Schor, C., Wood, I., & Ogawa, J. (1984). Binocular sensory fusion is limited by spatial resolution. *Vision Research, 24*(7), 661–665.
Serrano-Pedraza, I., & Read, J. C. (2009). Stereo vision requires an explicit encoding of vertical disparity. *Journal of Vision, 9*((4)3), 1–13. https://doi.org/10.1167/9.4.3.
Spang, K., Gillam, B., & Fahle, M. (2012). Electrophysiological correlates of binocular stereo depth without binocular disparities. *PLoS ONE, 7*(8), https://doi.org/10.1371/journal.pone.0040562.
Sprague, W. W., Cooper, E. A., Tosic, I., & Banks, M. S. (2015). Stereopsis is adaptive for the natural environment. *Science Advances, 1*(4), https://doi.org/10.1126/sciadv.1400254.
Tallon-Baudry, C., Bertrand, O., Delpuech, C., & Pernier, J. (1996). Stimulus specificity of phase-locked and non-phase-locked 40 Hz visual responses in human. *Journal of Neuroscience, 16*(13), 4240–4249.
Taulu, S., Kajola, M., & Simola, J. (2004). Suppression of interference and artifacts by the Signal Space Separation Method. *Brain Topography, 16*(4), 269–275.
Taulu, S., & Simola, J. (2006). Spatiotemporal signal space separation method for rejecting nearby interference in MEG measurements. *Physics in Medicine & Biology, 51*(7), 1759–1768. https://doi.org/10.1088/0031-9155/51/7/008.
Tsao, D. Y., Vanduffel, W., Sasaki, Y., Fize, D., Knutsen, T. A., Mandeville, J. B., ... Tootell, R. B. (2003). Stereopsis activates V3A and caudal intraparietal areas in macaques and humans. *Neuron, 39*(3), 555–568.
Tzourio-Mazoyer, N., Landeau, B., Papathanassiou, D., Crivello, F., Etard, O., Delcroix, N., ... Joliot, M. (2002). Automated anatomical labeling of activations in SPM using a macroscopic anatomical parcellation of the MNI MRI single-subject brain. *Neuroimage, 15*(1), 273–289. https://doi.org/10.1006/nimg.2001.0978.
Uka, T., & DeAngelis, G. C. (2004). Contribution of area MT to stereoscopic depth perception: Choice-related response modulations reflect task strategy. *Neuron, 42*(2), 297–310.
van Ee, R., & Erkelens, C. J. (1995). Binocular perception of slant about oblique axes relative to a visual frame of reference. *Perception, 24*(3), 299–314.
van Ee, R., & Erkelens, C. J. (1996). Temporal aspects of binocular slant perception. *Vision Research, 36*(1), 43–51.
van Ee, R., & van Dam, L. C. (2003). The influence of cyclovergence on unconstrained stereoscopic matching. *Vision Research, 43*(3), 307–319.
Voloh, B., & Womelsdorf, T. (2016). A role of phase-resetting in coordinating large scale neural networks during attention and goal-directed behavior. *Frontiers in Systems Neuroscience, 10*, 18. https://doi.org/10.3389/fnsys.2016.00018.
Wang, L., Mruczek, R. E., Arcaro, M. J., & Kastner, S. (2015). Probabilistic maps of visual topography in human cortex. *Cerebral Cortex, 25*(10), 3911–3931. https://doi.org/10.1093/cercor/bhu277.